

Figure 1

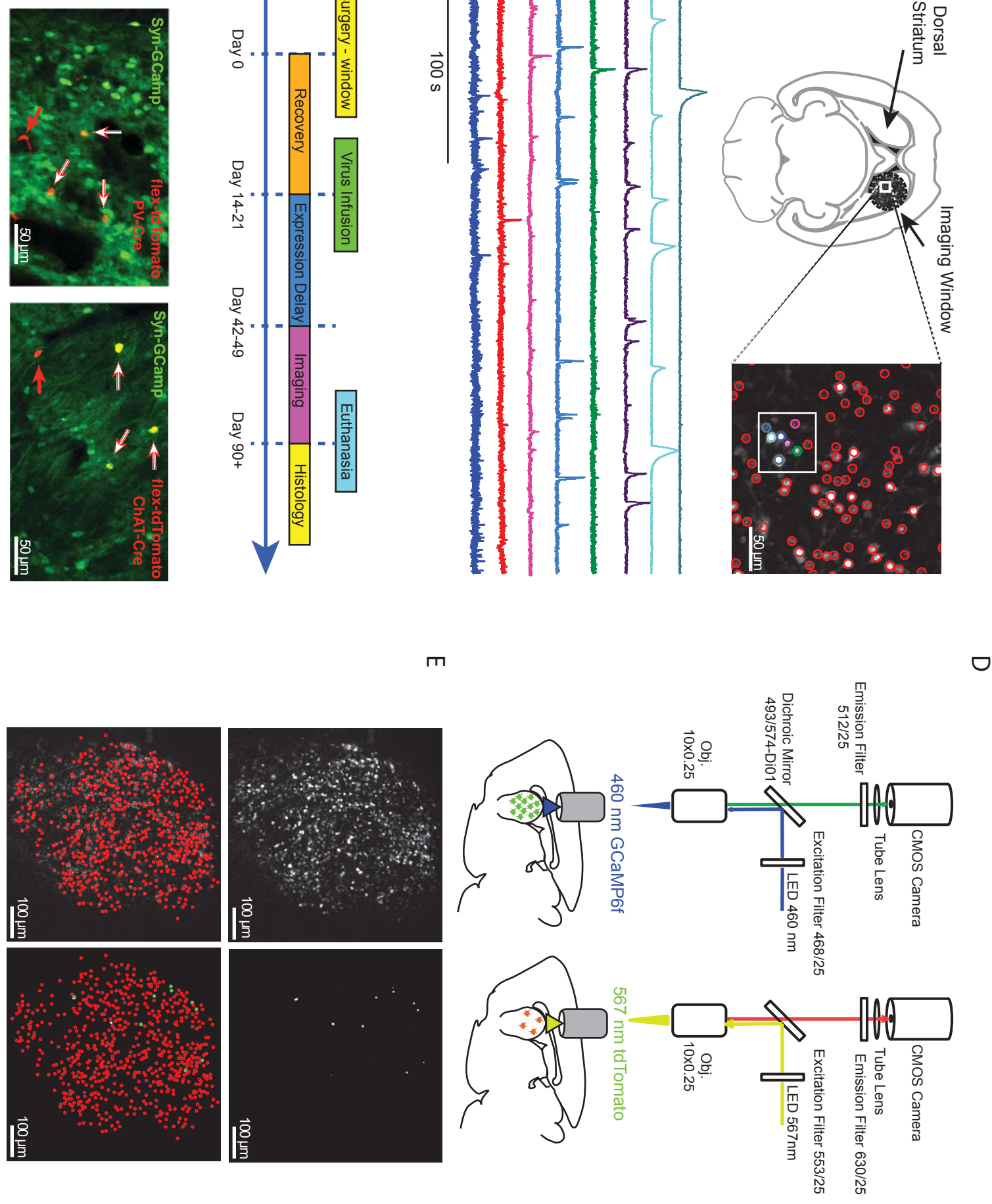


Figure 1: Experimental Paradigm and Imaging Protocol.

(A) Left, anatomical schematic showing imaging location in the striatum. Right, a representative fluorescence image showing GCaMP6f expressing neurons with manually identified regions of interest (ROI) corresponding to individual neurons used for calcium signal quantification. Fluorescence traces from individual neurons from a typical recording session are shown below in color corresponding to the label shown in the image above. **(B)** Experimental timeline. **(C)** Post-study histological photomicrograph showing GCaMP6 fluorescence (green) and Cre-dependent tdTomato fluorescence (red) from a representative animal. Red arrows indicate cells only expressing tdTomato. White arrows highlight cells co-expressing GCaMP6 and tdTomato. **(D)** Imaging setup and representative two channel imaging from a PV-cre mouse. Recording sessions began with calcium imaging of gCaMP6f in the dorsal striatum using a 460nm LED (left), followed with tdTomato imaging with a lime LED (567nm: right). **(E)** Wide-field images from each recording condition described in (D). Top, the GCaMP6 image represents max pixel intensity from all frames. Bottom, same GCaMP6 image as above with manually identified ROIs overlaid. Red circles indicate GCaMP6f expressing cells, while green circles indicate cells co-expressing GCaMP6f and tdTomato. Recording sessions yielded a large number of total neurons ($n=281.6\pm34.2$) with a substantially smaller number of interneuron cell types (CHIs: $n=5.1\pm1.1$; PV: $n=4.4\pm0.8$, mean \pm SEM)

Figure 2

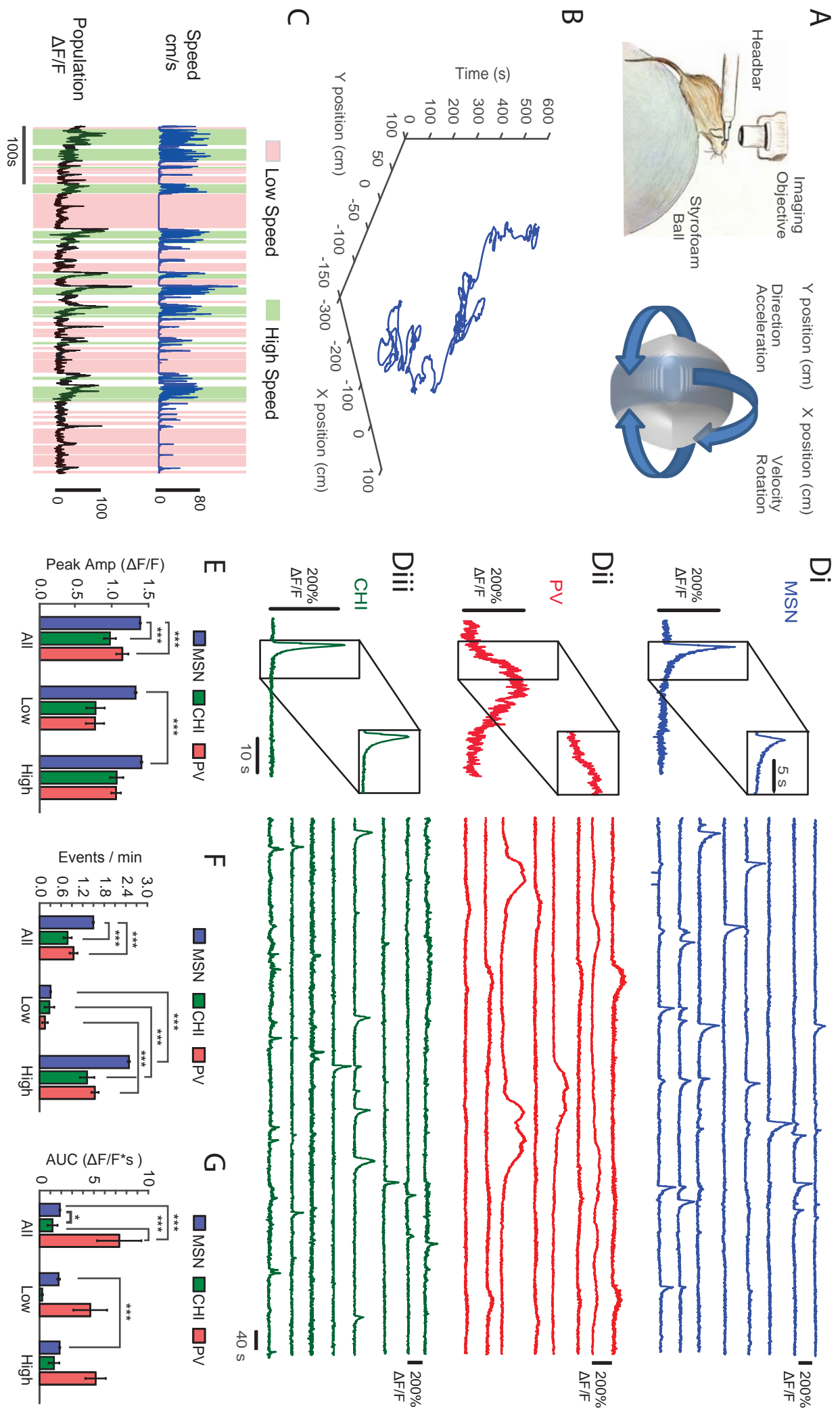


Figure 2: Motion Tracking and Striatal Cell Type Dynamics during Periods of Low and High Speed Movement.

(A) Schematic of behavioral paradigm showing head-fixed mouse under the imaging scope positioned on a spherical treadmill. The animal's current position and movement properties, including direction, linear and rotational velocity and acceleration can be assessed throughout the duration of the experiment. **(B)** A representative recording session with animal's location (x and y position) plotted over time. **(C)** Extracted movement speed (blue) and mean population GCaMP6 fluorescence (black) from the same recording session shown in B. Highlighting indicates periods of sustained high (green) or low speed movement (red). **(D)** Representative calcium events from the three populations of neurons recorded; MSNs (i), PV cells (ii) and CHIs (iii). **(E)** Calcium event peak amplitude during periods of high and low speed movement. Calcium event amplitude was greater for MSNs than CHIs and PVs, which were similar (Kruskal-Wallis, main effect of cell type, $X^2(2)=38.4$, $p<0.001$, $n_{\text{MSN}}=7727$, $n_{\text{PV}}=78$, $n_{\text{CHI}}=50$; Tukey's HSD post-hoc, MSN vs PV: $p<0.001$; MSN vs CHI: $p<0.001$; PV vs CHI: $p=0.35$; (high speed versus low speed; Sign-test, MSN: sign=682, $n=1798$, $p<0.001$; CHI: sign=5.0, $n=11$, $p=1$; PV: sign=6, $n=12$, $p=1$). **(F)** Event rates during high or low speed. Event rates for all neurons increased during periods of high speed, although MSN's showed the greatest change (Sign-test, MSN: sign=508, $n=7520$, 235 ties, $p<0.001$; CHI: sign=4, $n=47$, 4 ties, $p<0.001$; PV: sign=6, $n=73$, 6 ties, $p<0.001$) **(G)** Calcium event duration assessed as area under the curve, best dissociated the three cell types, with PVs' having the longest, and CHIs the shortest, event length (Kruskal-Wallis, $X^2(2)=37.3$, $p<0.001$, $n_{\text{MSN}}=7727$, $n_{\text{PV}}=78$, $n_{\text{CHI}}=50$; Tukey's HSD post-hoc, PV vs MSN: $p<0.001$, PV vs CHI, $p<0.001$)

Figure 3

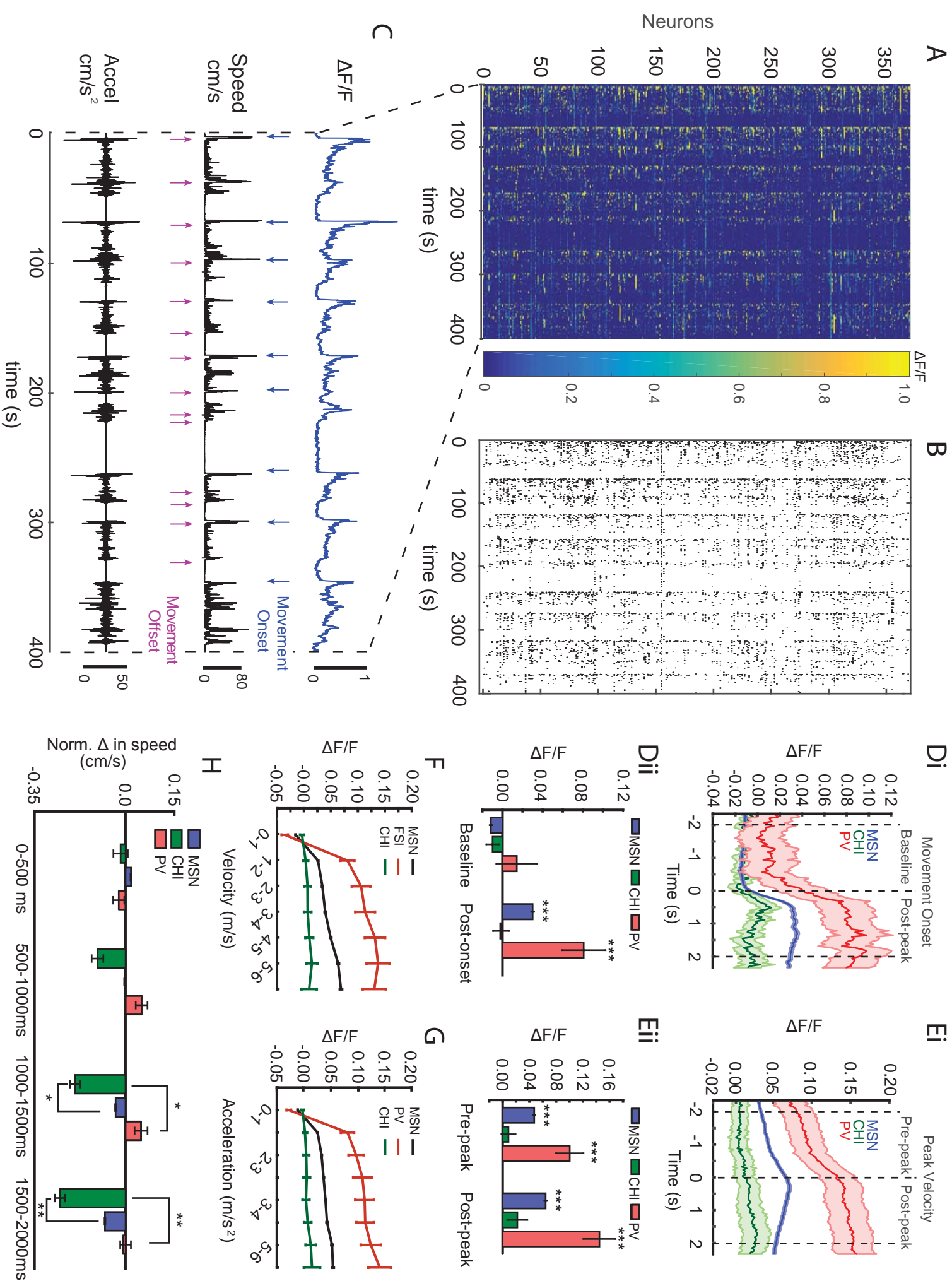


Figure 3: Striatal Population Activity Correlates with Discrete Aspects of Movement.

(A) A representative color map showing GCaMP6f activity from all 371 identified neurons recorded during a single 10 minute long imaging session. **(B)** Calcium traces of A, deconvolved into a binary “spike-like” signal. **(C)** Mean population GCaMP6f fluorescence (black:top), linear velocity (speed:blue), and acceleration from a typical session. Arrows indicate movement onset (blue) or movement offset (magenta). Onset and offset events were determined independently based on thresholded changes in movement over time (see methods). **(D)** Mean activity of each cell class relative to movement onset (i) and compared between the baseline and post onset window (ii). All cell classes showed an increase in mean fluorescence over baseline, except CHIs, coincident with movement onset (change from baseline; Sign-test, MSNs: sign=2515, n=7755 neurons, p<0.001; CHIs: sign=24, n=51 neurons, p=0.78; PVs: sign=15, n=79 neurons, p<0.001). **(E)** Mean population activity of each cell class relative to peak velocity (i) and quantification in the pre and post peak velocity windows (ii). MSNs and PV cells showed significantly higher fluorescence near peak velocity, while CHIs activity tended to peak as velocity began to decline (0 to ~2.0 seconds post-peak velocity vs pre-movement onset, Sign-test, MSN's: sign=2492, n=7755 neurons, p<0.001; PV's: sign=17, n=79 neurons, p<0.001; CHI's: sign=26, n=51 neurons, p=1). **(F)** Fluorescence signal of each cell class as a function of linear velocity. Only the activity in PV cells and MSNs was significantly correlated with changes in velocity (Friedman test, MSNs: $\chi^2(6)=3056$, p<0.001, n=7755; PV's: $\chi^2(6)=95.4$, p<0.001, n=79; CHIs: $\chi^2(6)=7.5$, p=0.28, n=51) **(G)** Fluorescence signal of each cell class as a function of acceleration. Fluorescence in PV and MSN cells, but not CHIs, was correlated with changes in acceleration (Friedman test, MSNs: $\chi^2(7)=3.33e+03$, p<0.001, n=7755; PV's: $\chi^2(7)=116$, p<0.001, n=79; CHI's: $\chi^2(7)=4.1$, p=0.77, n=51). **(H)** Changes in velocity centered on calcium events sorted by cell class. Significant changes in speed coincide with spike events in both CHI mice (Friedman test, main effect of time, $\chi^2(4) = 493$, p<0.001) and PV mice (Friedman test, main effect of time, $\chi^2(4) = 415$, p<0.001). PV calcium events were generally followed by increases in velocity, while CHI calcium events were followed by a decrease in locomotor output. Comparisons of time windows: 0-500ms (Kruskal-Wallis, $\chi^2(2)=3.3$, p=0.19); 500-1000ms (Kruskal-Wallis, $\chi^2(2)=5.4$, p=0.066); 1000-1500ms (Kruskal-Wallis, $\chi^2(2)=6.4$, p=0.04; Tukey's HSD post-hoc MSN vs CHI, p=0.048, PV vs CHI, p=0.041), 1500-2000ms (Kruskal-Wallis, $\chi^2(2)=12.8$, p<0.001; Tukey's HSD post-hoc MSN vs CHI, p=0.004, PV vs CHI, p=0.001).

Figure 4

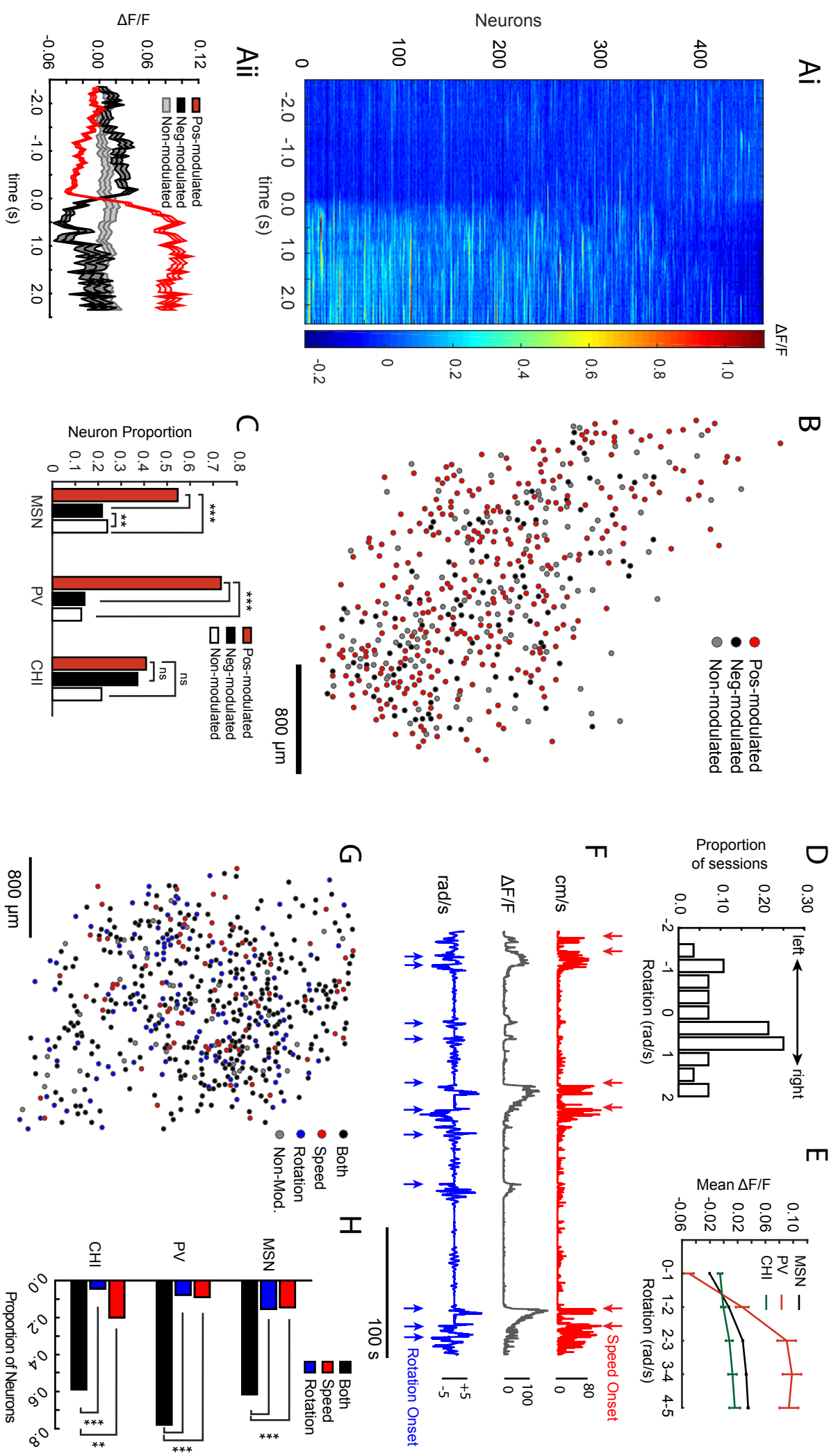


Figure 4: Heterogeneous Activity across all Three Cell Types Related to Movement.

(A) Neurons identified in a representative recording session, sorted by mean fluorescence (i; lowest: top, highest: bottom) and aligned to movement onset ($n=459$ neurons). Population activity of neurons classified as either positively, negatively, or non-modulated by movement onset (ii). **(B)** Anatomical distribution of neurons from the session shown in (A) that were positively modulated (red), negatively modulated (black), or non-modulated (gray). **(C)** Population histogram across all animals ($n=13$) showing proportion of neurons modulated by movement onset separated by polarity and cell type. **(D)** Animals showed no directional preference across imaging sessions, with an equal distribution of directional movement across sessions (difference in numbers of left-biased and right-biased sessions between CHI and PV mice: $X^2(1)=0.058$, $p=0.81$, Yates correction used). **(E)** Fluorescence signal of each cell class as a function of rotation calculated as angular velocity (Friedman, main effect of rotation, MSNs: $X^2(4)=3.20e+03$, $p<0.001$; PV's: $X^2(4)=1.17e+02$, $p<0.001$; CHI's: $X^2(4)=1.0e+01$, $p=0.04$). **(F)** Population activity relative to speed and rotation from a representative recording session. Speed onset and rotation onset periods are highlighted with arrows. **(G)** Neurons correlated with speed, rotation, or both from the animal depicted in (F) plotted anatomically. Neurons close together were likely to be related to the same aspects of motor output (Effect of distance by neuron category; Wilcoxon rank-sum, speed sensitive, $w_{\text{speed}}=4.64e+06$, $n_{\text{speed}}=1114$, $n_{\text{other}}=6524$, $p<0.001$; rotation: $w_{\text{rotation}}=4.96e+06$, $n_{\text{rotation}}=1114$, $n_{\text{other}}=6595$, $p<0.001$; conjunctive: $w=1.97e+07$, $n_{\text{conjunctive}}=4748$, $n_{\text{other}}=2961$, $p<0.001$). **(H)** Population histogram showing proportion of neurons correlated with velocity alone (red), rotation alone (blue) or both (black), sorted by cell type. All three cell types, were more likely to be both speed and rotation conjunctive than either alone (MSNs: $X^2(1)=2.2e+02$, $p<0.001$; PVs: $X^2(1)=4.2$, $p=0.039$ (yates correction); CHIs: $X^2(1)=9.61$, $p=0.002$ (yates correction)) (Bonferroni-corrected p-values). Number of conjunctive neurons differed significantly from speed alone: MSN's, $X^2(1)=2269$, $p<0.001$, CHI's, $X^2(1)=10$, $p=0.005$, PV's, $X^2(1)=43.8$, $p<0.001$ or rotation alone: MSN's, $X^2(1)=2150$, $p<0.001$, CHI's, $X^2(1)=24.5$, $p<0.001$, PV's, $X^2(1)=46.1$, $p<0.001$ (Bonferroni-corrected p-values).

Figure 5

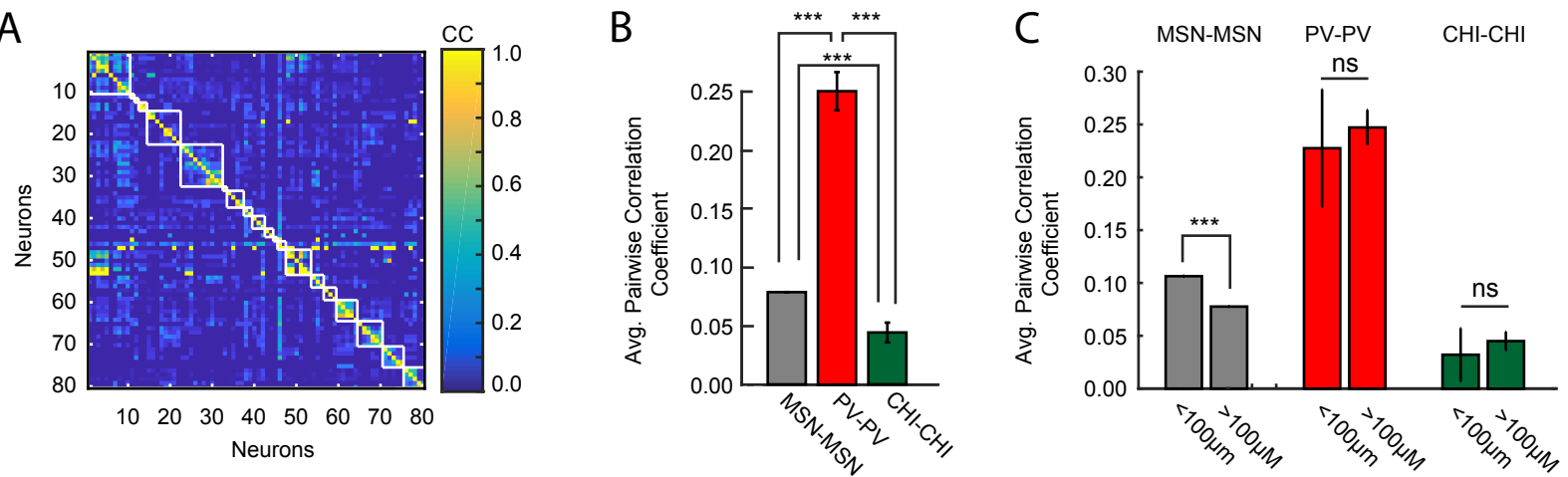


Figure 5: Anatomical Clustering of Coordinated Activity of Striatal Cell Types.

(A) Correlation matrix of 80 neurons from a representative recording session. White lines represent boundaries between unique neuron pairs within 100 μ m of one another (i). **(B)** Pairwise correlation between the same cell types during a representative recording session. PV cells showed the highest correlation values (Kruskal-Wallis, $X^2(2)=148$, $p<0.001$; Tukey's HSD post-hoc, MSN-MSN vs CHI-CHI: $p<0.001$; MSN-MSN vs PV-PV: $p<0.001$; PV-PV vs CHI-CHI: $p<0.001$). **(C)** Population histograms of pairwise correlation of each cell type across all animals sorted by distance. Unlike MSN pairs, correlated activity between interneurons was not modulated by distance (Effect of distance; Wilcoxon rank-sum, MSN-MSN pairs, $w_{<100}=5.3e10$, $n_{<100}=62895$, $n_{>100}=1429304$, $p<0.001$; PV-PV pairs: $w_{<100}=1955$, $n_{<100}=17$, $n_{>100}=224$, $p=0.7$; CHI-CHI pairs, $w_{<100}=684$, $n_{<100}=9$, $n_{>100}=143$, $p=1$).

Figure 6

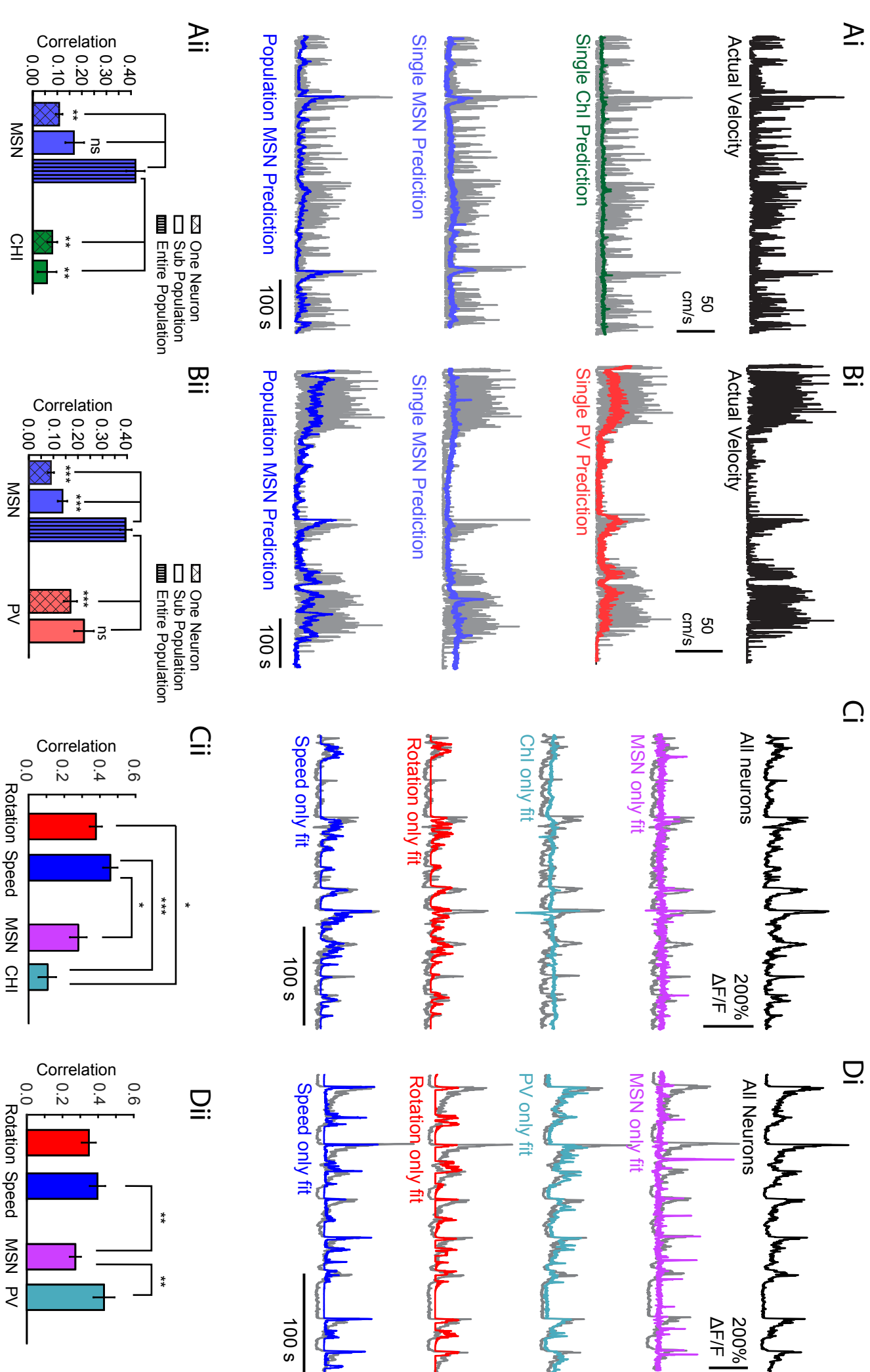


Figure 6: PV Cells, but not CHIs, are Strong Predictors of Motor State and the Striatal Population Code.

(A) Velocity prediction based on the activity of interneuron or MSN activity for a representative CHI mouse (i). Actual velocity of the mouse movement is plotted in black (top), and gray (bottom three) for comparison with predicted velocity using single CHIs (green), single MSNs (light blue) and population MSNs (dark blue). Quantification of the population predictor performance across all ChAT-cre mice (ii). Predictor performance, calculated as a regression coefficient, for an equal number of simultaneously recorded CHIs and MSNs in a given recording session, and averaged across sessions (Friedman test, main effect predictor type, ChAT-Cre mice, $\chi^2(4)=20.8$, $p<0.001$). Sub populations represent an equivalent number of MSNs as the full CHI population from each recording session ($n = 5.1 \pm 1.1$, mean \pm SEM). **(B)** Same as (A) except from a representative PV-cre mouse (i) and predictor performance quantification for all PV-cre mice (ii). Actual velocity of the mouse is in black. Predicted velocity based on the activity of a single PV neuron (red), a single MSN (light blue), or population MSNs (dark blue) are plotted superimposed on the actual velocity (gray). Sub populations represent an equivalent number of MSNs as the full PV population from each recording session ($n=4.6 \pm 0.86$ (mean \pm SEM); Friedman test, main effect predictor type; PV-cre mice, $\chi^2(4)=50.1$, $p<0.001$). **(C)** Actual population striatal neuron fluorescence (black, top, and gray in bottom four) and predicted fluorescence based on the activity of identified CHIs (green), or an equivalent number of MSN neurons (magenta) from a representative ChAT-cre mouse (i), and across all mice (ii). For comparison, predictions of population fluorescence was also made using motor output (rotation:red; speed:blue). Friedman test, $\chi^2(3) = 24$, $p<0.001$; post-hoc Tukey's HSD, speed vs. CHI: $p<0.001$; rotation vs CHI: $p=0.03$; MSN vs CHI, $p=0.16$. **(D)** Same as (C) except for PV neurons in PV-cre mice. Friedman test, $\chi^2(3)=16.7$, $p=0.001$; post-hoc Tukey's HSD, speed vs PV: $p=1$, rotation vs PV: $p=0.46$; PV vs. MSNs, $p=0.001$.

Figure 7

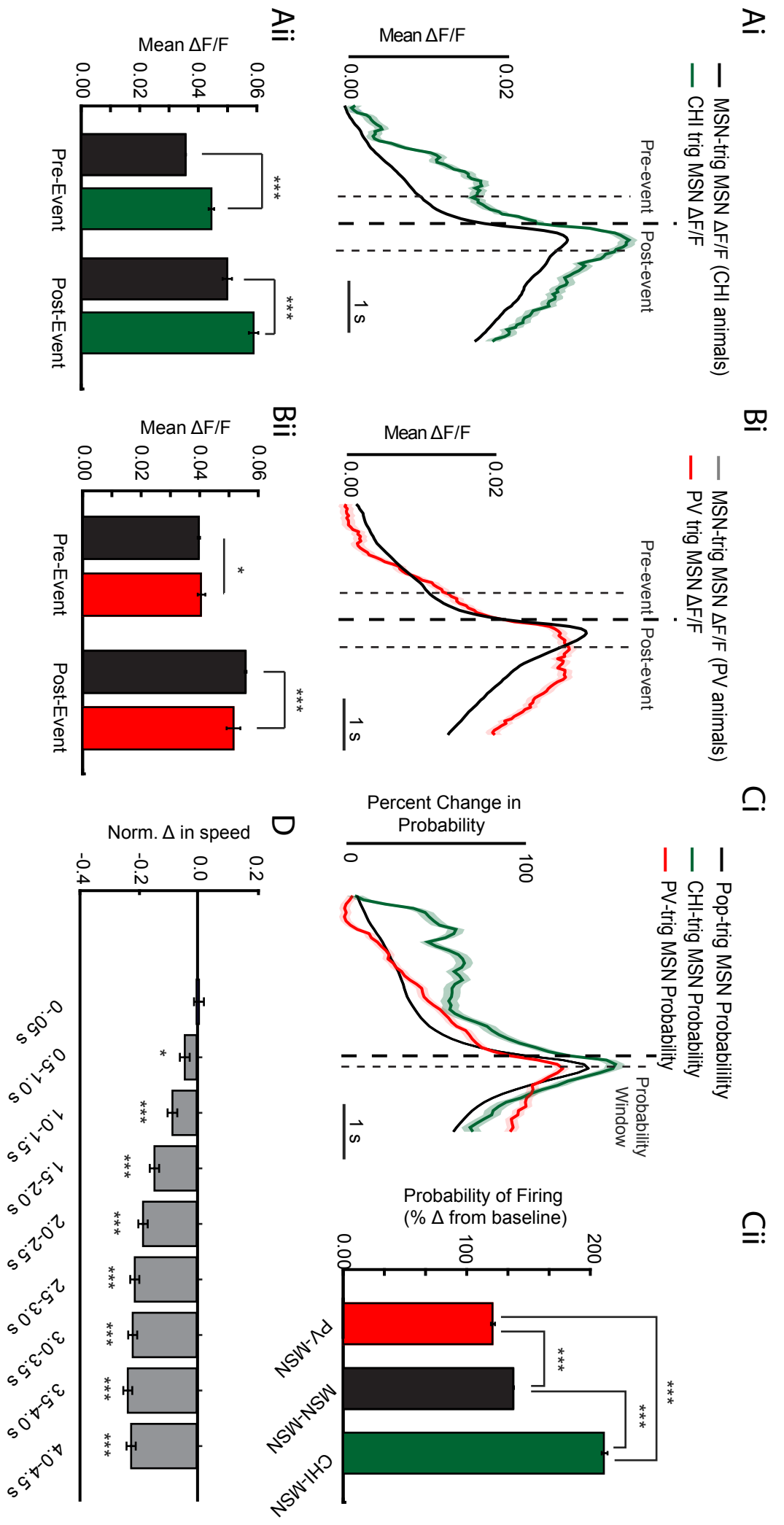


Figure 7: Interneurons Regulate MSN Activity and Network State.

(Ai) CHI calcium event-triggered MSN population fluorescence (green) versus MSN calcium event-triggered MSN population fluorescence (black) from all ChAT-Cre animals. MSN population fluorescence was significantly elevated prior to CHI calcium events compared to a MSN calcium event (CHI pre-event: Wilcoxon rank-sum, $w=1.72e+12$, $n_{\text{CHI}}=153680$, $n_{\text{MSN}}=22116844$, $p<0.001$), as well as after a CHI calcium event (CHI post-event: Wilcoxon rank-sum, $w=1.73e+12$, $p<0.001$, $n_{\text{MSN}}=22116844$, $n_{\text{CHI}}=153680$). **(Aii)** Quantification of MSN population fluorescence in the 500ms before (pre-event) and 500ms after (post-event) a CHI calcium event (green) shown in comparison to a MSN calcium event (black). **(B)** Same as (A) but for PV-cre mice. MSN median population fluorescence was lower both prior to and following a calcium PV event (PV pre-event: Wilcoxon rank-sum, $w=2.43e+12$, $n_{\text{PV}}=237528$, $n_{\text{MSN}}=20289773$, $p=0.034$; PV post-event: Wilcoxon rank-sum, $w=2.42e+12$, $n_{\text{PV}}=237528$, $n_{\text{MSN}}=20289773$, $p<0.001$). **(Ci)** Change in calcium event probability in MSNs following a MSN calcium event (black), a CHI calcium event (green), or a PV calcium event (red), in all animals. **(Cii)** Population histogram quantifying the change in probability in the 100ms following a calcium event. Coincident with a CHI calcium event, MSNs show an increase in event probability, whereas following a PV calcium event, MSNs show a decrease in event probability, relative to MSN event probability without interneuron events (Pairwise Z-tests, MSN-MSN vs PV-MSN, $z=-32.0$, $p < .001$; PV-MSN vs CHI-MSN, $z=-10.8$, $p<0.001$; MSN-MSN vs MSN-CHI, $z=31.4$, Bonferroni corrected post-hoc for multiple comparisons, $*p<0.001$). Changes were calculated as a percent change in probability from the baseline spike rate (Bonferroni corrected post-hoc for multiple comparisons ($*p<0.001$)). **(D)** Peak probability triggered changes in velocity. Population velocity binned into 500ms windows following identified peaks in the probability of activity (see methods). (Friedman test, main effect of time, $X^2(8)=520$, $p<0.001$; Tukey's HSD post-hoc, (vs 0-0.5 s) 0.5-1 seconds, $p=0.027$, 1.00-4.50 seconds, all $p<0.001$; $^{*}=p<0.05$, $^{***}p<0.001$).

Figure S1

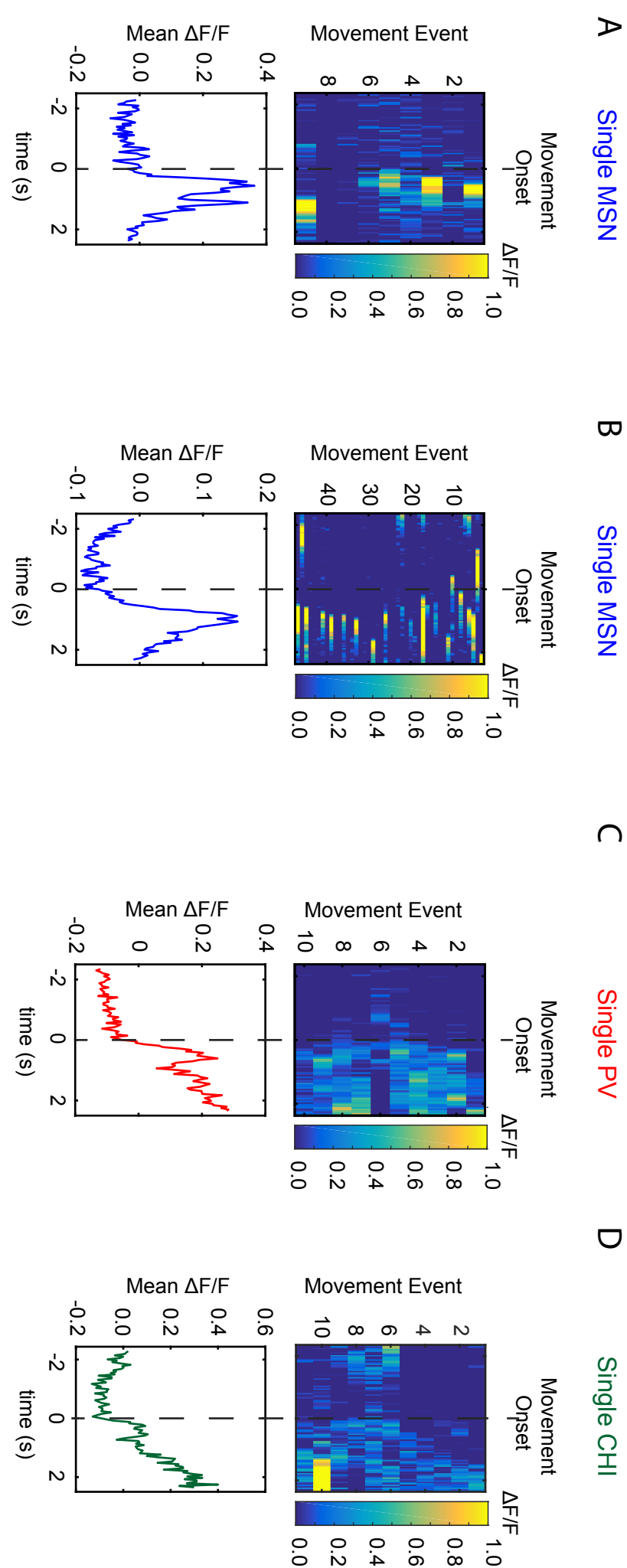
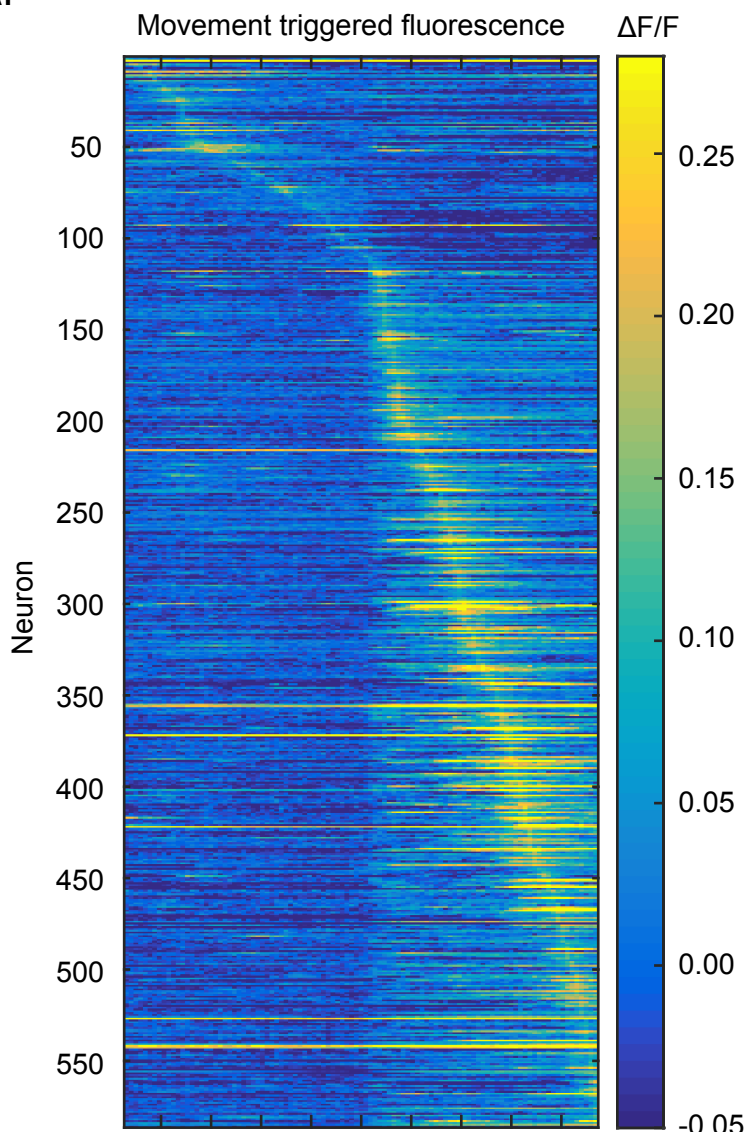
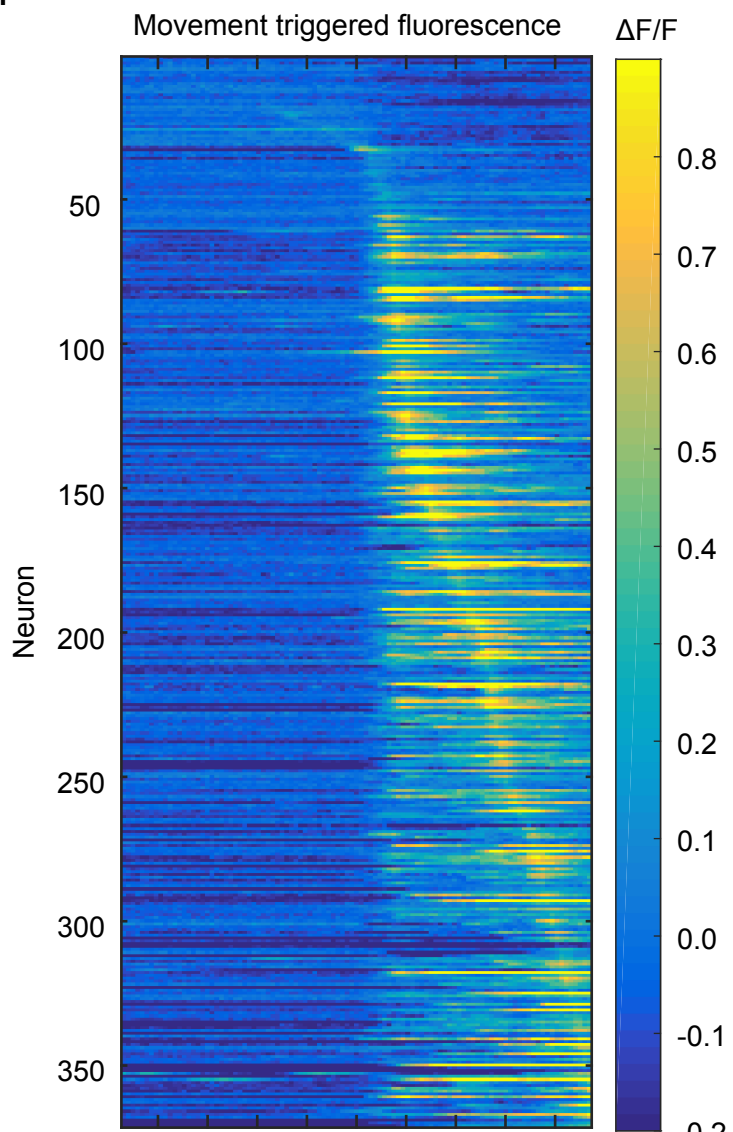


Figure S2

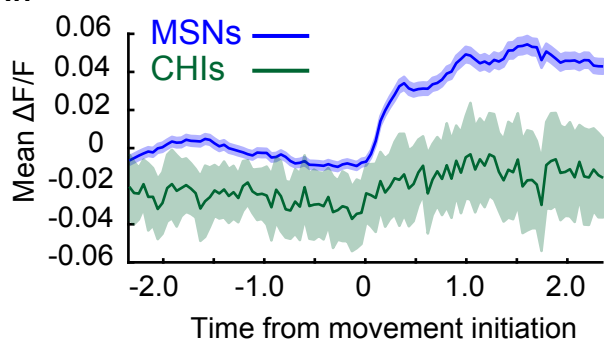
Ai



Bi



Aii



Bii

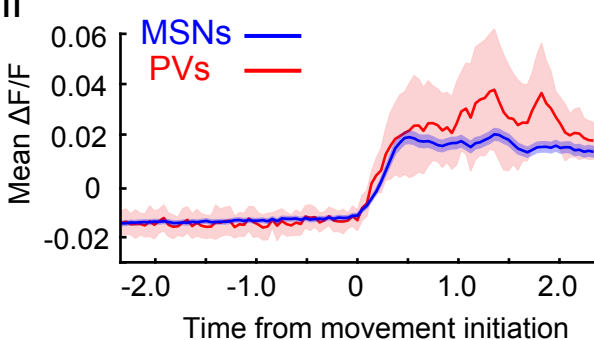
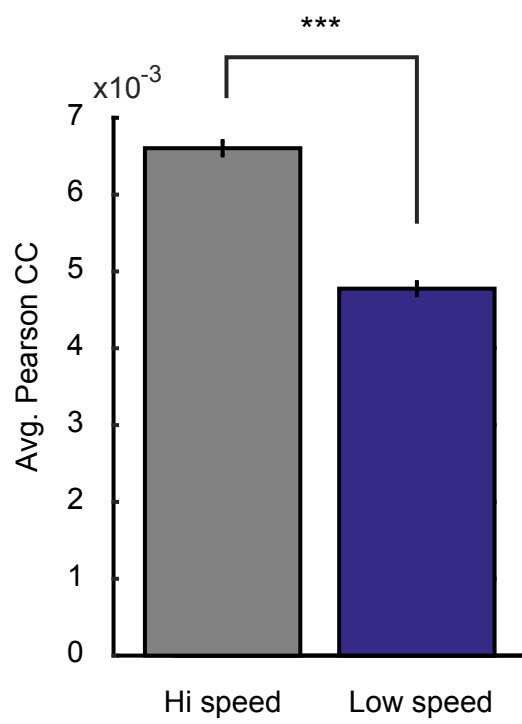


Figure S3

A

ROI Correlation Strength



B

Difference in (Hi - Low) Correlation Strength by distance

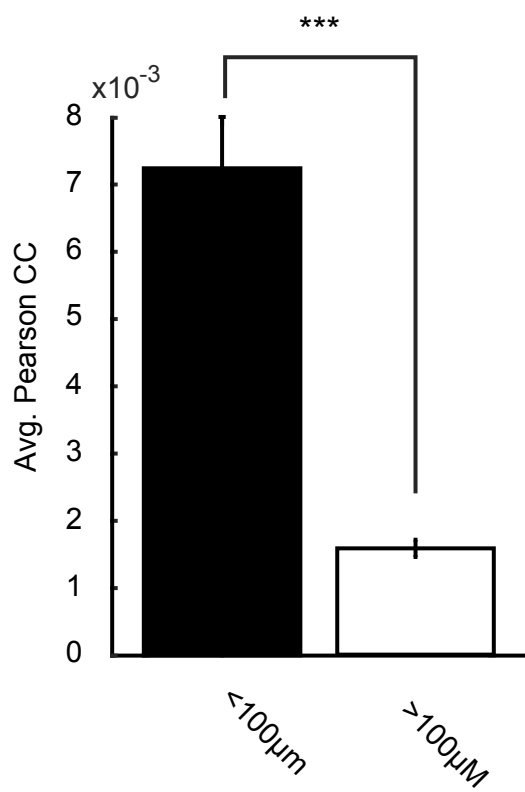


Figure S4

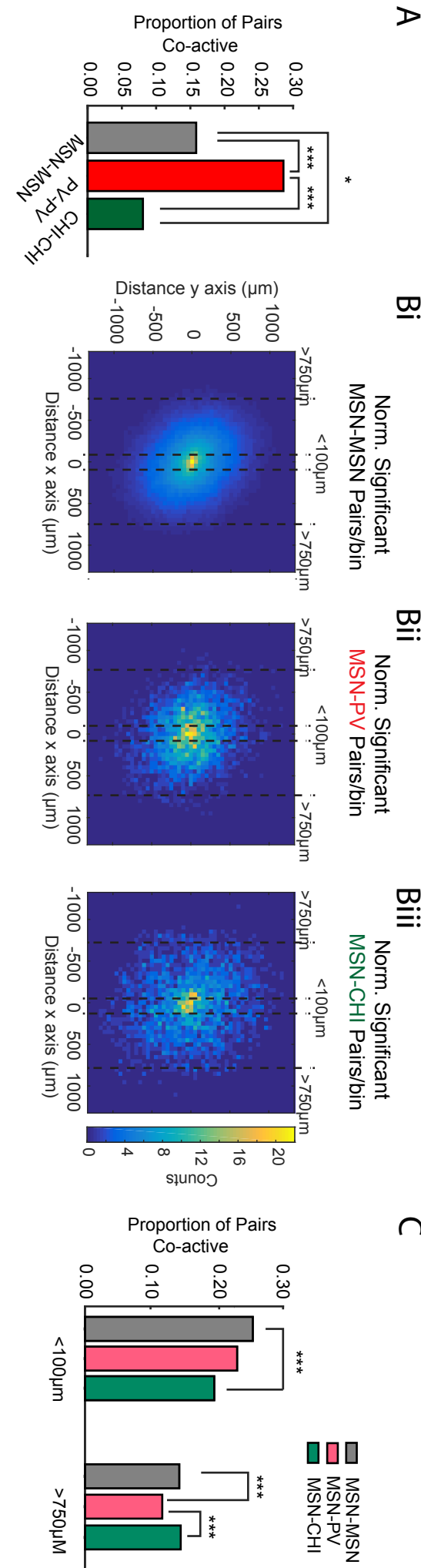


Figure S1: Individual Neuron Variability at Movement Onset.

(A, B) Representative MSN activity aligned at movement onset for all trials, in two different recording sessions from two different animals. **(C)** Representative PV activity aligned at movement onset, sorted by trial, from a typical recording session and typical animal. **(D)** CHI activity aligned at movement onset from a representative Chat-Cre animal.

Figure S2: Movement Triggered Fluorescence Changes in all Cells Recorded from a Representative PV-Cre mouse and a Representative ChAT-Cre mouse.

(A) Colormap presents fluorescence intensity across all recorded neurons from a representative ChAT-Cre animal, sorted by average fluorescence intensity of a cell within 5 seconds of movement onset (i). Population average of movement triggered fluorescence from non-cholinergic neurons (blue) and identified (green) cholinergic neurons across all cholinergic mice (ii). **(B)** Same as (A) but for a representative PV-Cre animal (i), and across all PV animals (ii).

Figure S3: Coordinated Activity Changes during Movement.

(A) Population histograms showing pairwise correlation strength between periods of high and low speed (Wilcoxon sign rank, $w=5.78e+11$, $p<0.001$, $n=1502053$). **(B)** Difference in correlation strength between high and low speed periods separated by anatomical distance across all cells (Wilcoxon rank sum, $<100\mu ms$ vs $>100\mu ms$; $w_{<100}=4.88e+10$, $p<0.001$, $n_{<100}=63219$, $n_{>100}=1438834$).

Figure S4: Pair-wise Co-activation Plotted over Anatomical Distance and by Cell Type.

(A) Population histograms for all animals showing proportion of significantly correlated pairs sorted by cell class. PVs and MSNs show significantly more correlation between neurons within the same class (MSNs vs. CHIs: $X^2(1)=8.4$, $p=0.01$; PVs vs. CHIs: $X^2(1)=26.0$, $p<0.001$). **(B)** Population colormaps from all animals showing significantly correlated cell pairs sorted by distance. MSN-MSN cell pairs (i) and MSN-Interneuron cell pairs (PV, ii; CHI, iii). Interneuron-MSN pairs differ from MSN-MSN pairs in that MSN-CHI cells are correlated over greater distances than MSN-MSN pairs and MSN-PV are correlated over smaller distances than MSN-MSN pairs (MSN-MSN median = $411\mu ms$, MSN-PV: $343\mu ms$, MSN-CHI: $448\mu ms$; Kruskal-Wallis, $X^2(2)=305$, $n_{MSN-MSN}=238155$, $n_{MSN-PV}=4021$, $n_{MSN-CHI}=2679$, $p<0.001$; Tukey's HSD post-hoc, MSN-PV vs MSN-MSN: $p<0.001$, MSN-PV vs MSN-CHI: $p<0.001$, MSN-MSN vs MSN-CHI: $p<0.001$). **(C)** Population histograms for all animals showing proportion of significantly correlated MSN-interneuron pairs sorted by near and far distances. The number of significantly correlated pairs is greater for MSN-MSN pairs under $100\mu m$ than it is for MSN-CHI pairs: ($X^2(2)=17.6$, $p<0.001$; Bonferroni-corrected pairwise comparison, MSN-MSN vs MSN-CHI: $X^2(1)=14.6$, $p<0.001$). The number of significantly correlated MSN-MSN, and MSN-CHI pairs is greater over $750\mu m$ than it is for MSN-PV pairs: ($X^2(2)=18.6$, $p<0.001$; Bonferroni-corrected pairwise comparison, MSN-MSN vs MSN-PV: $X^2(1)=18.5$, $p<0.001$, MSN-PV vs MSN-CHI: $X^2(1)=12.9$, $p<0.001$).